# Experimental loss rates due to emission from Ne, Ar, and Xe ions at high plasma densities

T. J. Baig* and H.-J. Kunze

*Institut für Experimentalphysik V, Ruhr-Universität, 44780 Bochum, Federal Republic of Germany*
(Received 23 June 1992)

Neon, argon, and xenon gases were introduced at small impurity concentrations to high-density hydrogen plasmas produced in a gas-liner pinch. The electron density and temperature as well as the impurity densities were obtained as a function of time by laser scattering. Energy considerations allowed the derivation of radiative-energy-loss coefficients for the three elements in the temperature range from 5 to about 20 eV at electron densities of about $10^{24}$ m$^{-3}$. The influence of the density is clearly seen when comparing different discharges; higher densities result in lower losses. Furthermore, losses are increasing as the temperature decreases, instead of decreasing.

## I. INTRODUCTION

The power radiated by multiply ionized atoms is an important issue in laboratory and astrophysical plasmas. It represents a critical loss term, which has to be reduced as much as feasible in some applications, for others it is being deliberately optimized. Magnetically confined plasmas produced for thermonuclear fusion are the most investigated example of the first category [1,2]. Discharges driven by pulsed high-power electric generators and used as powerful radiation sources are typical of the second category [3]. Another example are high-density laser-produced plasmas, where radiation losses are desired as a means for rapid cooling to achieve population inversion for soft x-ray lasers [4,5].

The energy loss from plasmas by radiation occurs through several channels, and the important physical processes are line emission, radiative recombination, dielectronic capture followed by line emission, and bremsstrahlung. It is customary to express these losses in terms of *radiative-energy-loss coefficients* $p$ [6] (radiative-power-loss function or cooling rate are also used for this quantity in the literature), i.e., power radiated per ion and per electron. In general, the total radiative loss coefficient $p_{tot}$ is a function of electron temperature and electron density for each atomic species, since each contribution ($p_1$ due to line radiation, $p_r$ due to radiative recombination, $p_d$ due to dielectronic recombination, and $p_b$ due to bremsstrahlung) depends on the fractional abundances of the ionic species. Only in the coronal limit, where collisional transitions between atomic levels become small and the fractional abundances are independent of the electron density, are all energy-loss coefficients functions solely of the electron temperature.

In this coronal limit, loss coefficients have been calculated for a number of elements by several authors. It became evident that losses due to line emission always dominate by at least an order of magnitude [7–10], until the $K$ shell is being substantially ionized. For the present experiment it suffices, therefore, to consider only this loss channel.

Most authors restricted their calculations to elements of interest essentially to nuclear fusion. Post *et al.* [11] obtained losses due to line radiation for 47 elements employing the "average ion model" for steady-state plasmas. The uncertainty was expected to be a factor 2–4 and even larger for high-$Z$ elements at low temperatures. Summers and McWhirter [10] were able to quote an uncertainty of ±50% for their calculations since they used better data. They also cite extensively the relevant literature.

Zhu *et al.* [12] were the first to report experimental radiation losses for iron ions by measuring absolutely the emission of about 50 lines from a $\theta$-pinch plasma.

With increasing electron density collisions become important; population densities have to be calculated using a collisional-radiative model and the ionic abundances are determined by their respective collisional-radiative rate coefficients. A thermodynamic equilibrium (LTE) model becomes adequate only for very high densities. Electron collisions shift the ionization balance and reduce the population densities through collisional deexcitation. As a consequence, radiative loss coefficients decrease generally with increasing electron density. Detailed studies have been carried out for aluminum plasmas by Duston and Davies [13] and by Keane and Skinner [14] for oxygen. Gerusov used an approximate hydrogenlike model for neon [15], and Galushkin and Kogan did their calculations for plasmas containing berylliumlike to hydrogenlike ions [16].

At high densities, radiative transport will certainly influence the radiation losses, and the assumption of an optically thin plasma limits the maximum allowed plasma dimension [15]. In transient plasmas, finally, the changing ionic abundances have to be properly taken into account [14].

## II. EXPERIMENTAL SETUP AND THOMSON SCATTERING

The investigations of radiation losses were carried out on the gas-liner pinch, which has been described in detail by Finken and Ackermann [17] and by Kunze [18]. In principle, it is a large-aspect-ratio gas-puff $z$ pinch (the

electrodes are 18 cm in diameter and 5 cm apart) with two independently operated fast electromagnetic valves. Through the outer valve the main gas (for the present experiments it was always hydrogen) is introduced and forms initially a thin hollow cylinder along the inner surface of the evacuated glass chamber. It is preionized by discharging a 50-nF capacitor (charged to 20 kV) through 50 needles arranged annularly underneath the lower electrode, that communicate with the main chamber through a mesh in the electrode surface. A discharge current from a 11.1-$\mu$F capacitor bank charged to 35 kV accelerates the initial plasma towards the axis, where the final pinch plasma is formed.

The second fast valve makes it possible to independently puff in impurity gases along the axis of the discharge chamber. The amount can be controlled by varying the pressure in the respective plenum and to some extent also by adjusting the opening time of the valve with respect to the outer one. For the present investigations the injection times were selected such that the impurity ions were distributed evenly within the plasma column. The impurities were neon, argon, and xenon gases, each with three different concentrations.

The plasma parameters were studied by 90° collective Thomson scattering employing a $Q$-switched ruby laser (model K-1Q) at 694.3 nm; it delivered a laser pulse of 3.0 J with a duration of 30 ns. In order to resolve the narrow central peak due to the heavy impurity ions in the spectrum of the scattered light, special attention was paid in all alignment procedures to minimize the spectral width of the laser and especially the width of the apparatus profile of the detection system. The power of the laser pulse and its timing was monitored by a FND-100 photodiode, which was placed behind the beam dump. The continuum radiation of the plasma was monitored in a 10-nm band centered at 520 nm with an RCA Model 1P28 photomultiplier at the exit slit of a $\frac{1}{4}$ m monochromator.

The light scattered by the plasma was focused onto the entrance slit of a 1 m monochromator (Spex model 1704) employing a 1:1 imaging optics. The plane grating of 1200 lines/mm was blazed at 1000 nm and hence the spectrum could be recorded in second order with an optical-multichannel-analyzer system (OMA II) positioned in the exit plane of the instrument. It was gated for about 90 ns. The reciprocal dispersion of this arrangement was 0.0063 nm/channel, and the apparatus profile was obtained from Rayleigh scattering of the laser in propane as well as with the help of a neon spectral lamp; it had a full width at maximum (FWHM) of 0.025 nm.

The determination of plasma parameters by scattering of laser light [19,20] is a well-established diagnostic technique for laboratory plasmas. For high-density low-temperature plasmas, the scattering parameter $\alpha$ usually is larger than 1 ($\alpha \gg 1$) and the scattering spectrum has a width characteristic of the velocity of the ions. An analysis of all details of this "ion component" of the spectrum, however, allows the derivation of the electron temperature and the ion temperature as well as the electron density if only one species of ions is present in the plasma

[21]; the approximation by Salpeter [22] is employed for this. An admixture of small amounts of impurity ions modifies the ion component, and these effects have been studied theoretically by Evans [23]. If a heavy-ion impurity is introduced into a light-ion plasma, the principal effect is to superimpose an additional narrow peak, the total intensity of which is proportional to the density of the added impurities. Kasparek and Holzhauer [24] have observed such spectra from plasmas containing two different types of ions, but a systematic experimental study of the admixture of impurities has been carried out only recently by DeSilva et al. [25,26] employing the very same experimental setup as used in the present investigations. A typical example of a spectrum is shown in Fig. 1. The narrow ion feature of the argon ions is superimposed on the broad profile due to the motion of the protons. The FWHM of this central peak yields essentially the temperature of the impurity ions; its intensity scales with the square of their mean charge and linearly with its density [26]. Temperature and density of the main plasma component are correspondingly proportional to the width and the area of the broad spectrum, respectively.

As Fig 1 shows, all single-shot spectra are obtained highly resolved with details. Careful analysis of the shapes without impurities revealed that electron and ion temperatures of the hydrogen plasma were practically equal. By fitting theoretical profiles of Evans [Eq. (3) of Ref. [23]] to the experimental ones, it was possible to derive electron temperature $T_e$ of the main plasma, temperature of the impurity ions $T_{imp}$, electron density $n_e$ and impurity density $n_{imp}$, or the mean charge $\langle Z \rangle$ of the impurity species from each individual spectrum. For this fitting procedure, theoretical profiles were convoluted with the apparatus profile. Since the impurity peak is
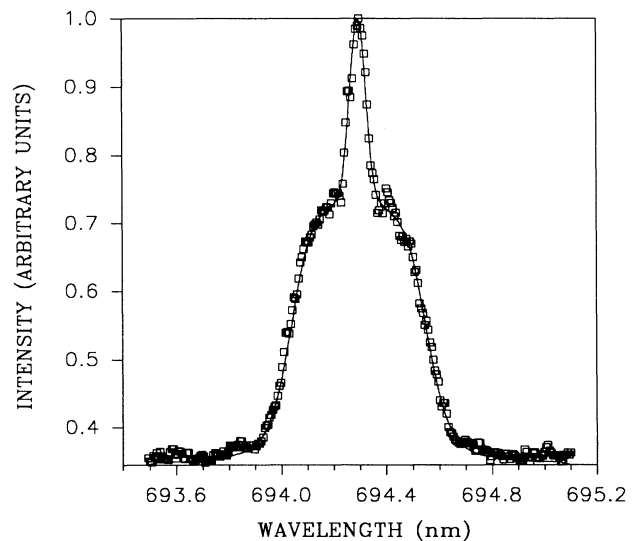


FIG. 1. Example of line profile of scattering radiation obtained at $t = 125$ ns after maximum compression. The plasma parameters derived are $T_e = 15.0$ eV, $T_{imp} = 14.0$ eV, $\langle Z \rangle = 3.6$, $n_e = 0.7 \times 10^{24}$ m$^{-3}$, $n_{imp} = 1.6 \times 10^{22}$ m$^{-3}$.
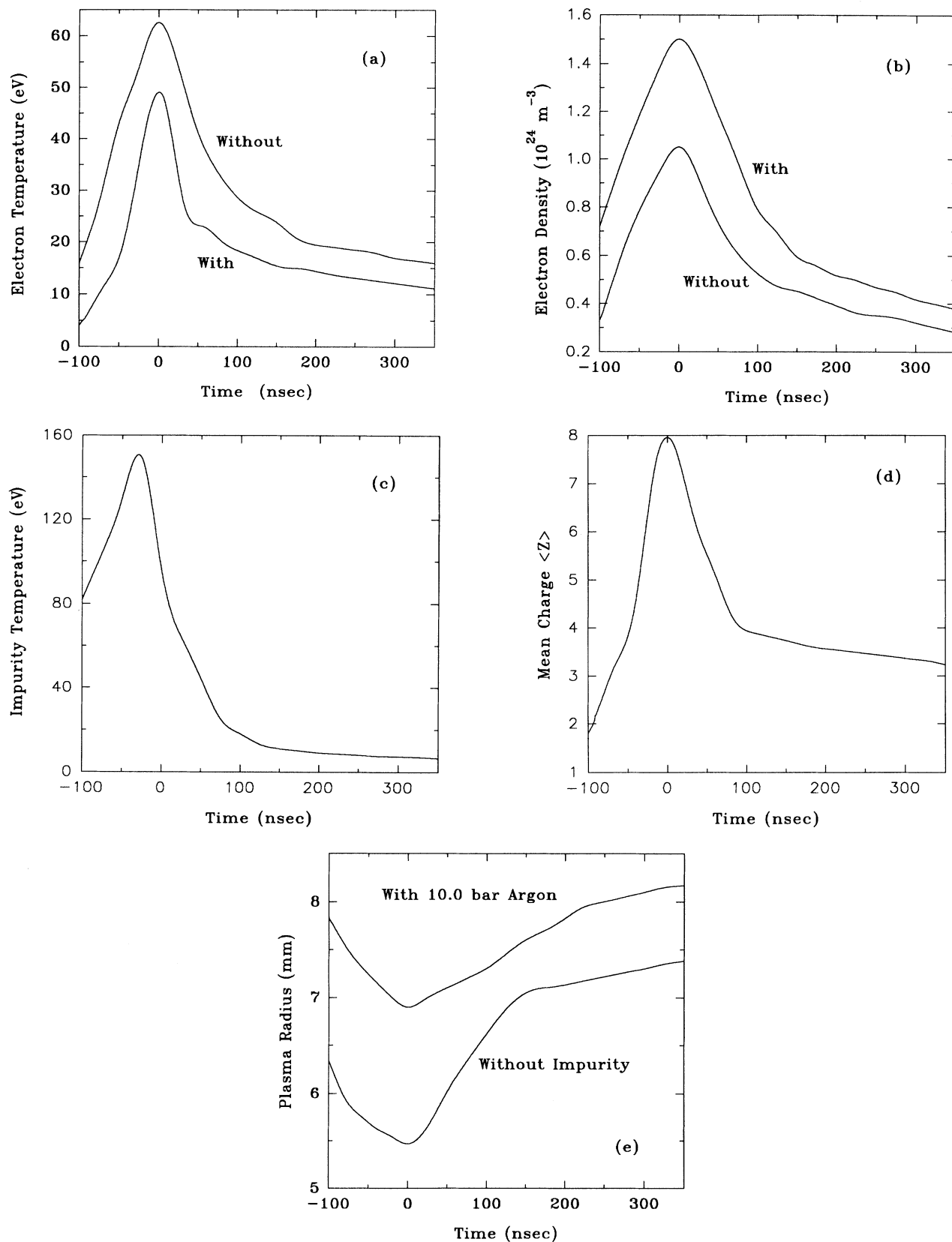
FIG. 2. Time evolution of plasma parameters for discharges without impurities and with argon (5.0 bars Ar in the plenum of the fast valve): (a) electron temperature; (b) electron density; (c) impurity temperature; (d) mean charge; (e) plasma radius.

proportional to $n_{imp}\langle Z \rangle^2$, either $n_{imp}$ must be known or $\langle Z \rangle^2$ must be obtained from different considerations in order to obtain the other quantity. In ionization equilibrium, $\langle Z \rangle$ is a function of temperature and density, and if the low-density limit is applicable, it is a sole function of the temperature. In this limit, $\langle Z \rangle$ can be deduced, for example, from the calculations of Arnaud and Rothenflug [27]. However, in a strongly ionizing phase of the plasma, $\langle Z \rangle$ will be lower than the equilibrium value, and in a recombination phase it will be higher. At the time of maximum compression we assumed, therefore, ionization equilibrium (ionization times being shortest at the highest densities and temperatures), calculated $\langle Z \rangle$ from Ref. [27] employing the experimental temperature, and thus determined $n_{imp}$. We used this impurity density for all other times before and after maximum compression, assuming a constant mixing ratio of the impurity species in the plasma. In this way $\langle Z \rangle$ was obtained for all other times without any further assumption.

The spatial emission of the plasma column was studied in the midplane by imaging the cross section of the plasma column onto the entrance slit of the monochromator (width 30 $\mu$m, height 2.0 cm) such that the radial intensity distribution of the plasma was along the height of the slit. The image at the exit slit thus reflected the radial intensity distribution at a selected wavelength. It was recorded with the optical multichannel analyzer (OMA II) aligned such that the diode array was also along the height of the slit. The spatial resolution was given by the width (25 $\mu$m) of the diodes. The radial emission was recorded for various times during the discharge and for plasmas with and without added impurities.

For the observation of neon and argon the Ne III line at 267.79 nm was observed in fourth order and the Ar IV line at 291.3 nm in second order. The height of each diode of 2.5 mm corresponded to a spectral width of 0.32 nm in second order and assured that the total line was recorded. The emission without impurities was recorded at the same wavelength intervals. This emission was solely continuum radiation. No suitable line in the visible was found for higher ionization stages of Xe, and we take the radius found for Ar also for the case with Xe. For different concentrations of Ne, the radius of the plasma column was practically the same as without impurity, whereas with Ar it was larger by about 2.0 mm. Different plasma parameters in discharges with and without impurity are a consequence of an early impurity gas injection: the impurity gas spreads and influences the compression dynamics. Hydrogen is fully ionized in all cases.

Figure 2 shows the time evolution of plasma parameters for the pure hydrogen discharge and for one impurity case as an example: electron temperature (a), electron density (b), impurity temperature ($T_{imp}$) (c), mean charge of the impurity (d), and plasma radius (e).

## III. RADIATIVE-POWER-LOSS CALCULATIONS

We assign the subscript 0 to all quantities of the plasma when there are no impurities introduced, and the subscript $i$ to those cases with impurities in the plasma.

### A. Plasmas with no impurities

The power balance equation for a completely ionized hydrogen plasma of volume $V_0$, when there is no power loss other than by bremsstrahlung and recombination radiation and by heat transfer to the electrodes, can be written as

$$\frac{d}{dt}\left[\frac{3}{2}nkT_{e0}V_0\right] = P_{in0} - P_{b0} - P_{r0} - P_E , \qquad (1)$$

where $n$ is the total particle density $(n = n_{e0} + n_{i0} = 2n_{e0})$ for a fully ionized hydrogen plasma, $T_{e0}$ is the average electron temperature $(T_{e0} = T_{i0}$ is derived from the
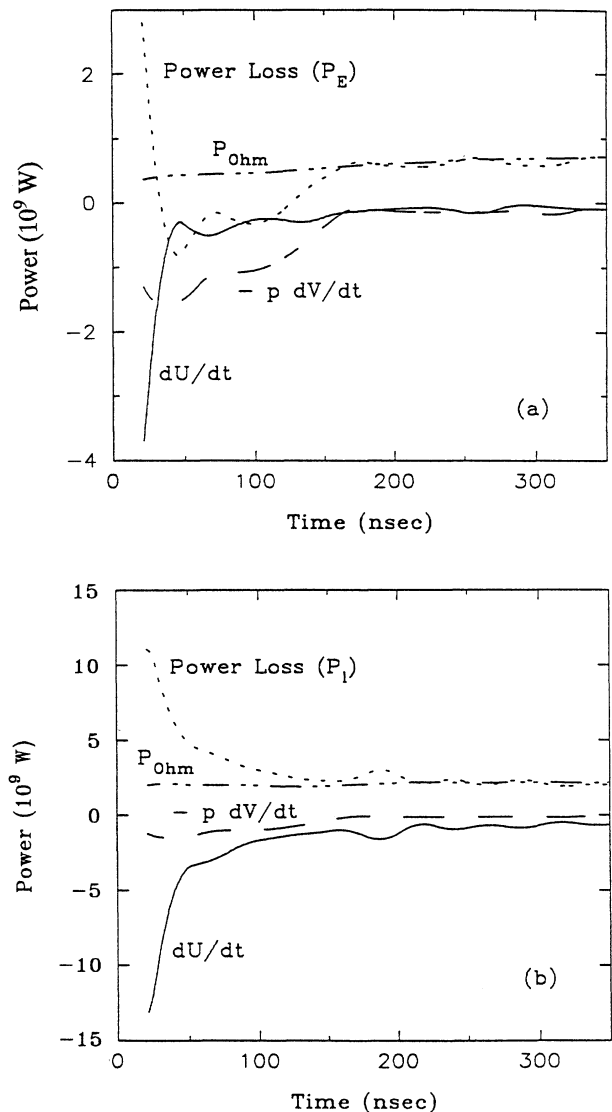


FIG. 3. Ohmic heating $P_{Ohm}$, rate of charge of the internal energy $dU/dt$ and work done on the magnetic field $p\,dV/dt$, power loss to the electrodes $P_E$ and power loss by line radiation $P_l$; (a) discharge with no impurity, (b) discharge with 2.5 bars neon in the plenum of the fast wave.

analysis of scattered light spectra). $V_0 = \pi r_0^2 l$, where $r_0$ is the radius of the plasma column and $l$ its length. The term on the left-hand side of Eq. (1) represents the rate of change of the internal energy of the plasma, and the second and third term on the right-hand side are the power radiated by bremsstrahlung $P_{b0}$ and by recombination radiation $P_{r0}$. The first term on the right-hand side is the total input power, which is the sum of Ohmic heating, the initial kinetic energy of the implosion, and the work done on (by) the contracting (expanding) pinch by (on) the magnetic field $B$ at the pinch boundary. The last term $P_E$ is the power loss due to heat transfer to the electrodes of the discharge chamber.

The power $P$ in watts emitted by bremsstrahlung and recombination radiation as given by Griem [6] is

$$P_{b0} = 1.69 \times 10^{-38} n_{e0}^2 (kT_{e0})^{1/2} V_0 \; ,$$

$$P_{r0} = 2.4 \left[ \frac{E_H}{kT_{e0}} \right] P_{b0} \; , \tag{2}$$

where the electron density $n_{e0}$ is in $\mathrm{m}^{-3}$, the electron temperature $kT_{e0}$ in eV, and the plasma volume $V_0$ in $\mathrm{m}^3$. We can calculate the unknown power loss to the electrodes from Eq. (1) after maximum compression once the initial kinetic energy of the implosion has been thermalized:

$$P_E = -3 \frac{d}{dt}(n_{e0} k T_{e0} V_0) - \frac{\mu_0 l}{4\pi} \frac{I^2}{r_0(t)} \frac{dr_0}{dt}$$

$$+ \eta \frac{I^2 l}{\pi r_0^2} - P_{b0} - P_{r0} \; , \tag{3}$$

where $\eta$ is the Spitzer resistivity. We assume homogeneous Ohmic heating of the plasma since the skin depth is of the order of the radius of the plasma column.

## B. Plasma with impurities

The power balance equation with some impurity can be written as

$$\frac{d}{dt} \left[ \frac{3}{2} [(n_{ei} + n_{pi})kT_{ei} + n_{imp}kT_{imp}] V_i + n_{imp} E_{ion} V_i \right]$$

$$= P_{ini} - P_{tot} - P_E \; , \tag{4}$$

where $n_{pi}$ is the proton density and $E_{ion}$ is the total ionization energy of one ionic species, i.e., the sum of the
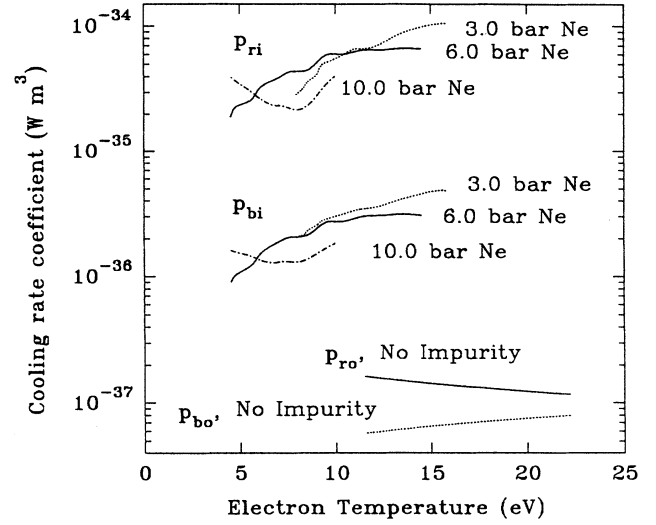


FIG. 4. Rate coefficients for cooling by bremsstrahlung $p_b$ and recombination radiation $p_r$ for cases with no impurity (0) and with neon (i) added.

ionization energies up to the charge state $Z$ multiplied with the fraction $f$ of the ions in this charge state,

$$E_{ion} = \sum_i \left[ f_i \sum_{z=0}^{z-1} E_{zi} \right] \; . \tag{5}$$

The quantity in the large square brackets of Eq. (4) represents again the internal energy $U$. The total radiated power $P_{tot}$ is

$$P_{tot} = P_l + P_b + P_r + P_d \; , \tag{6}$$

where $P_l$ is the power loss due to line radiation, $P_b$ to bremsstrahlung, $P_r$ to radiative recombination, and $P_d$ to dielectronic recombination. For the present plasma conditions $P_d$ can be neglected.

We now take the power loss to the electrodes $P_E$ to be the same in both cases with and without impurities and use an effective $Z_{eff}$ for the calculation of $P_b$, $P_r$, and the Ohmic heating. For $P_b$, for example, we have

$$P_{bi} = 1.69 \times 10^{-38} n_{ei} (\langle Z \rangle^2 n_{imp} + n_{pi})(kT_{ei})^{1/2} V_i \; . \tag{7}$$

The line radiation thus becomes

$$P_l = -\frac{d}{dt} \left[ \frac{3}{2} [(n_{ei} + n_{pi})kT_{ei} + n_{imp}kT_{imp}] V_i + n_{imp} E_{ion} V_i \right] - \frac{\mu_0 l}{4\pi} \frac{I^2}{r_i(t)} \frac{dr_i}{dt} + \eta \frac{I^2 l}{\pi r_i^2} - P_{bi} - P_{ri} - P_E \; , \tag{8}$$

and the radiative-energy-loss coefficient due to line radiation in $\mathrm{W\,m}^3$ is obtained from

$$p_l = \frac{P_l}{n_{ei} n_{imp}} \; . \tag{9}$$

## IV. RESULTS AND DISCUSSION

We now employ the experimental parameters to calculate the individual terms of the power balance equations. Figures 3(a) and 3(b) show, for example, the results of

discharges without and with neon impurity for one impurity concentration where the impurity gas pressure in the plenum of the fast valve is quoted for identification of the discharge condition. Thomson scattering spectra confirm for discharges without impurity injection that no considerable amounts of other impurities from the walls or the electrodes were present. If there had been, they would be accounted for in the loss term $p_E$.

Figure 3(a) reveals that the internal energy $U$ changes rapidly after maximum compression at $t = 0$ ns. If the unknown power loss $P_E$ is calculated according to Eq.

(3), it too changes rapidly and assumes unreasonable values. The conclusion is simple. After maximum compression the plasma is not in equilibrium with the magnetic field and has to relax first; it thermalizes and expands for about 40 ns till quasisteady equilibrium with the confining field is established. Considerations of the power balance according to Eq. (4) are therefore meaningful only after that time. Figure 3(b) shows the corresponding loss and heating rates for one discharge with neon impurity: $P_l$ represents the power loss through line radiation obtained by Eq. (4), after contributions by bremsstrahlung and recombination radiation have been subtracted. These contributions have been calculated
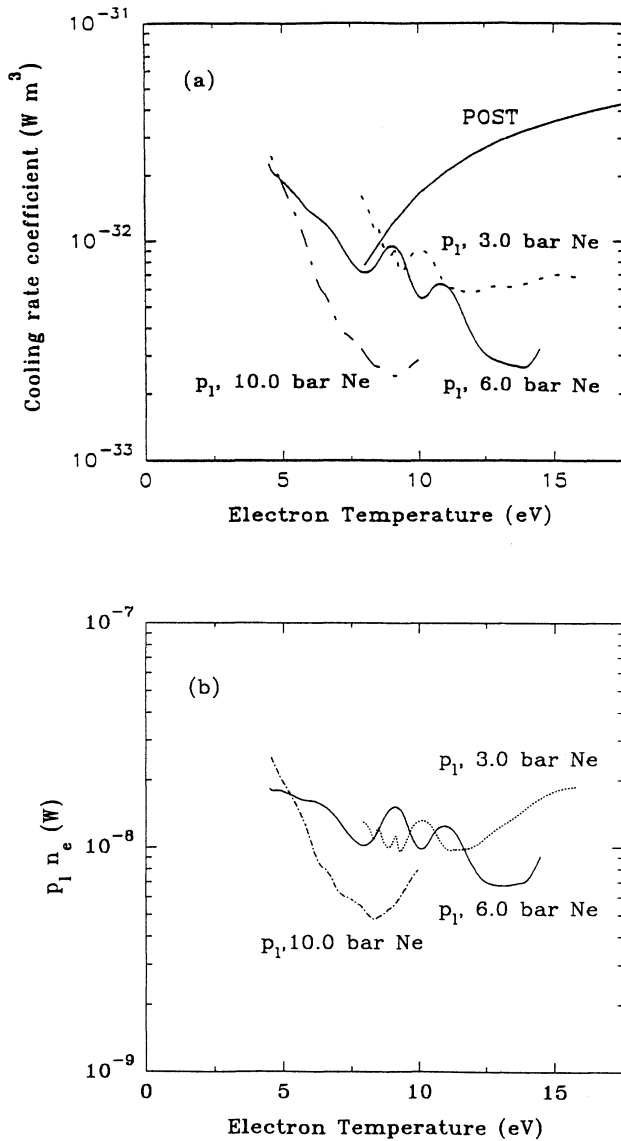


FIG. 5. (a) Cooling rate coefficient for neon derived from three discharges with different neon concentrations (3.0, 6.0, and 10.0 bars filling pressure in the plenum of the fast valve, which corresponds to impurity concentrations of 2.0%, 2.5%, and 3.3%, respectively, obtained from Thomson scattering). (b) $p_l n_e$ for neon.
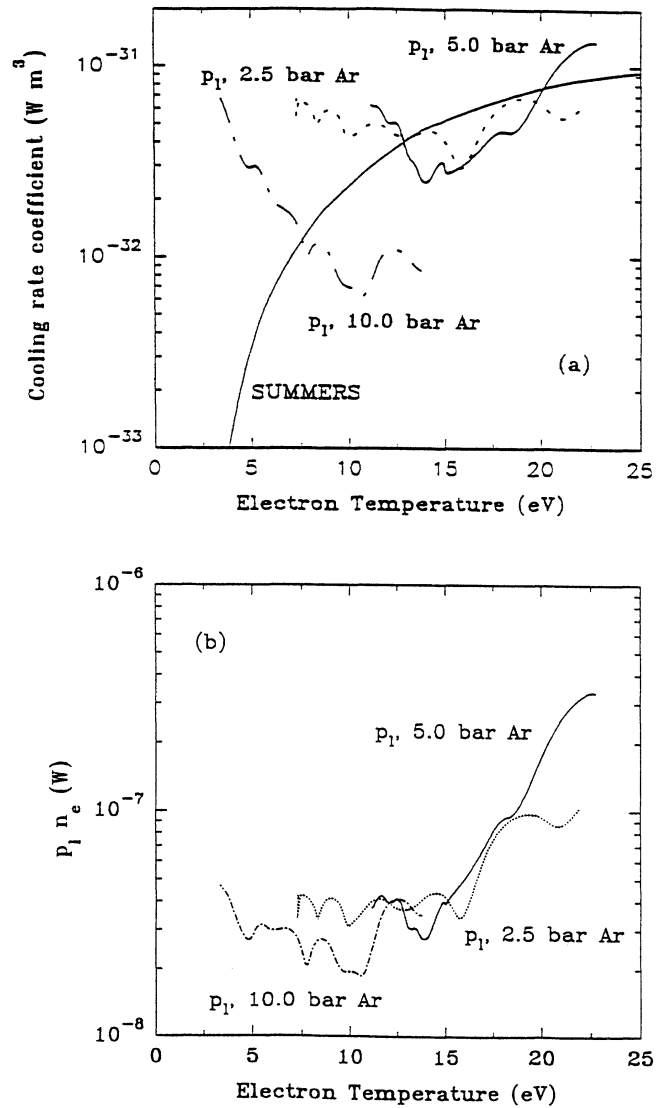
FIG. 6. (a) Cooling rate coefficient for argon derived from three discharges with different argon concentrations (2.5, 5.0, and 10.0 bars filling pressure in the plenum of the fast valve, which corresponds to impurity concentrations of 0.3%, 1.3%, and 0.6%, respectively). (b) $p_l n_e$ for argon.

with the experimental plasma parameters, and their magnitude is illustrated in Fig. 4 for the different discharge conditions. It is evident that line radiation indeed is the main loss mechanism and that the derived experimental loss rate may be interpreted accordingly. Figure 5(a) now shows the loss rate coefficient for line radiation. For comparison, the low-density loss rate coefficient calculated by Post et al. [11] is included. At about $T_e \cong 7$ eV their value agrees with the experimental values of the two cases with the lower impurity concentration; the electron density is $1 \times 10^{24}$ m$^{-3}$. The losses decrease towards higher temperatures and apparently with increasing impurity concentration. However, this can be a density

TABLE I. Radiative-energy-loss coefficients for neon obtained from different discharge conditions.

| $kT_e$ (eV) | $n_e$ ($10^{24}$ m$^{-3}$) | $p_l$ ($10^{-33}$ W m$^3$) |
|---|---|---|
| 15 | 2.6 | 6.4 |
| 12.5 | 1.9 | 6.5 |
| 10 | 1.4 | 8.0 |
| 7.5 | 0.7 | 20 |
| | | |
| 15 | 3.1 | 2.7 |
| 12.5 | 2.3 | 3.8 |
| 10 | 1.8 | 6.4 |
| 7.5 | 1.4 | 9.5 |
| 5.0 | 0.9 | 19 |
| | | |
| 10 | 2.7 | 2.5 |
| 7.5 | 1.6 | 3.6 |
| 5.0 | 1.1 | 19 |

effect as mentioned in the Introduction, since during the discharge higher densities are correlated with higher temperatures, and discharges with higher impurity concentration usually also have higher densities.

For a density of $10^{24}$ m$^{-3}$, Gerusov [15] quotes a reduction of the loss rate coefficient for neon by a factor between 6 and 9 in comparison with the low-density value. For oxygen this factor is even larger [14]. In order to elucidate this density effect, we calculated the product of loss rate coefficient and density ($p_l n_e$), since Keane and Skinner [14] predict a density variation proportional to $1/n_e$ for high densities. Figure 5(b) shows the result. For the temperature range from $T_e = 5$ to 15 eV all three cases yield a value of $p_l n_e \cong 1 \times 10^{-8}$ W to within a factor of 2, which corresponds to a loss rate coefficient for neon of

$$p_l \cong 1 \times 10^{-32} \text{ W m}^3 \text{ at } n_e \cong 10^{24} \text{ m}^{-3}, \ T_e = 5\text{--}15 \text{ eV}.$$

TABLE II. Radiative-energy-loss coefficients for argon obtained from different discharge conditions.

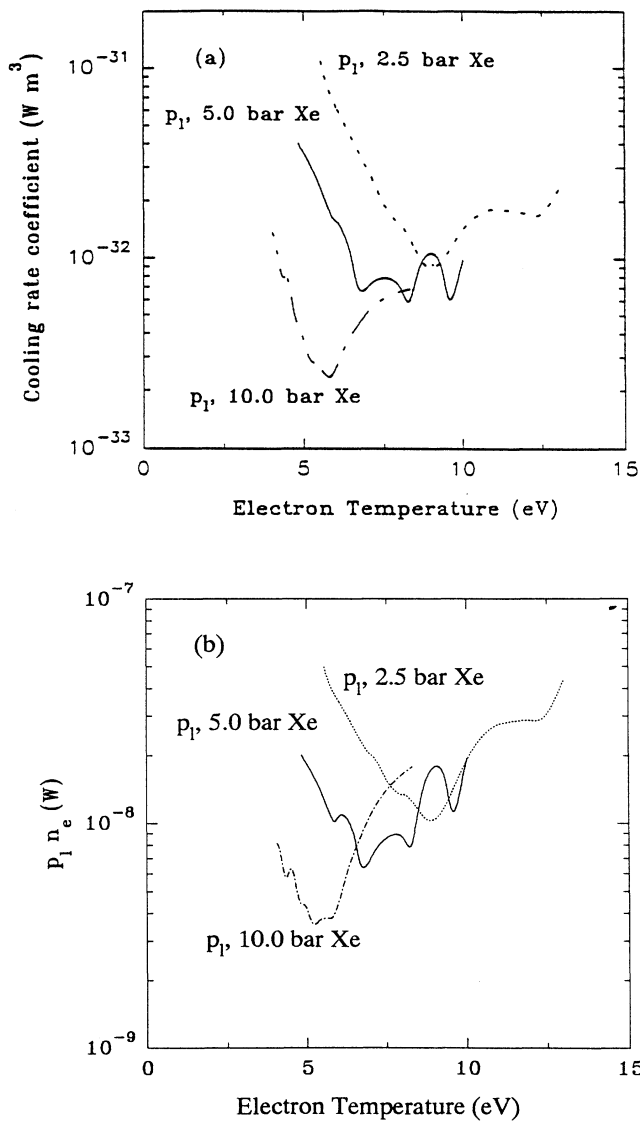| $kT_e$ (eV) | $n_e$ ($10^{24}$ m$^{-3}$) | $p_l$ ($10^{-32}$ W m$^3$) |
|---|---|---|
| 22.5 | 1.8 | 7.0 |
| 20 | 1.5 | 5.7 |
| 17.5 | 1.3 | 4.8 |
| 15 | 1.1 | 4.2 |
| 12.5 | 0.9 | 4.4 |
| 10 | 0.8 | 4.9 |
| 7.5 | 0.6 | 6.1 |
| | | |
| 22.5 | 1.1 | 13.3 |
| 20 | 0.9 | 7.4 |
| 17.5 | 0.7 | 4.2 |
| 15 | 0.6 | 2.9 |
| 12.5 | 0.45 | 4.5 |
| | | |
| 10 | 2.7 | 0.9 |
| 7.5 | 1.9 | 1.3 |
| 5.0 | 0.8 | 3.1 |



FIG. 7. (a) Cooling rate coefficient for xenon derived from three discharges with different xenon concentrations (2.5, 5.0, and 10.0 bars filling pressure in the plenum of the fast valve, which corresponds to impurity concentrations of 0.06%, 0.1%, and 0.4%, respectively). (b) $p_l n_e$ for xenon.

TABLE III. Radiative-energy-loss coefficients for xenon obtained from different discharge conditions.

| $kT_e$ (eV) | $n_e$ ($10^{24}$ m$^{-3}$) | $p_l$ ($10^{-32}$ W m$^3$) |
|---|---|---|
| 12.5 | 1.8 | 1.7 |
| 10 | 1.3 | 1.4 |
| 7.5 | 0.8 | 1.9 |
| 10 | 2.0 | 0.8 |
| 7.5 | 1.1 | 0.7 |
| 7.5 | 2.3 | 0.6 |

The error bars on the curves of Figs. 5–7 are estimated to be a factor of 2. If the above value is corrected for the density effect (a factor between 6 and 9), Post's value is obtained to within a factor of 2, at $T_e = 15$ eV; however, the true loss rates are much higher than the low-density value at lower temperatures.

Figures 6(a) and 6(b) show the results for argon; the low-density values of Summers and McWhirter [10] are included. All three cases give consistent results for the product $p_1 n_e$. It is nearly constant between 5 and 15 eV, and it increases strongly from 15 to 20 eV. Both results for neon and argon thus substantiate the predicted density dependence of $p_l$ at higher densities.

Again, when corrected for the density effect, the loss rates for argon will be higher than the theoretical low-density values, the discrepancy increasing towards lower temperatures.

Figures 7(a) and 7(b) show the results for the three discharges with xenon. The loss rates are consistent for about 9 eV. They differ, however, by more than a factor of 10 at lower temperatures. We suggest that this most likely is due to optical thickness, since the impurity concentration increases by a factor of 7 between the discharge conditions. No theoretical calculations are available for xenon.

The graphs of Figs. 5(a)–7(a) finally were smoothed and the experimental energy-loss coefficients with an estimated accuracy of a factor of 2 are summarized in Tables I–III. They are given for various temperature and density combinations realized in the experiment.

## ACKNOWLEDGMENTS

*Permanent address: Department of Physics, Quaid-I-Azam University, Islamabad, Pakistan.

[1] R. F. Post, Rev. Mod. Phys. 28, 338 (1956).

[2] W. B. Thompson, S. F. Edwards, J. Hubbard, and S. J. Roberts, in Proceedings of the Second United Nations International Conference on the Peaceful Use of Atomic Energy, edited by J. H. Martens et al. (United Nations, Geneva, 1958), Vol. 32, p. 65.

[3] Dense Z-Pinches, edited by N. R. Pereira, J. Davies, and N. Rostoker, AIP Conf. Proc. No. 195 (AIP, New York, 1989).

[4] J. C. Moreno, S. Goldsmith, H. R. Griem, L. Cohen, R. Epstein, D. Bradley, P. A. Jaanimagi, and J. Knauer, Phys. Rev. A 40, 4564 (1989).

[5] C. J. Keane and S. Suckewer, J. Opt. Soc. Am. B 8, 201 (1991).

[6] H. R. Griem, in Handbook of Plasma Physics, edited by M. N. Rosenbluth and R. Z. Sagdeev (North-Holland, Amsterdam, 1983), Vol. 1, p. 73.

[7] C. Breton, C. De Michelis, and M. Mattioli, Nucl. Fusion 16, 891 (1976).

[8] J. Davis, V. L. Jacobs, P. C. Kepple, and M. Blaha, J. Quant. Spectros. Radiat. Transfer 17, 139 (1977).

[9] C. Breton, C. De Michelis, and M. Mattioli, J. Quant. Spectros. Radiat. Transfer 19, 367 (1978).

[10] H. P. Summers and R. W. P. McWhirter, J. Phys. B 12, 2387 (1979).

[11] D. E. Post, R. V. Jensen, C. B. Tarter, W. H. Grasberger, and W. A. Lokke, At. Data Nucl. Data Tables 20, 397 (1977).

[12] Z. Y. Zhu, J. S. Wang, E. J. Iglesias, K. C. Maffei, and H. R. Griem, Nucl. Fusion 23, 1686 (1983).

[13] D. Duston and J. Davis, Phys. Rev. A 23, 2602 (1981).

[14] C. Keane and C. H. Skinner, Phys. Rev. A 33, 4179 (1986).

[15] A. V. Gerusov, Fiz. Plazmy 12, 106 (1986) [Sov. J. Plasma Phys. 12, 60 (1986)].

[16] Yu. I. Galushkin and V. I. Kogan, Nucl. Fusion 11, 597 (1971).

[17] K. H. Finken and U. Ackermann, Phys. Lett. 25A, 278 (1981); J. Phys. D. 15, 615 (1982); 16, 773 (1983).

[18] H.-J. Kunze, in Spectral Line Shapes, edited by R. J. Exton (Deepak, Hampton, VA, 1987), Vol. IV.

[19] J. Sheffield, Plasma Scattering of Electromagnetic Radiation (Academic, New York, 1975).

[20] H.-J. Kunze, in Plasma Diagnostics, edited by W. Lochte-Holtgreven (North-Holland, Amsterdam, 1968).

[21] A. Gawron, S. Maurmann, F. Böttcher, A. Meckler, and H.-J. Kunze, Phys. Rev. A 38, 4737 (1988).

[22] E. E. Salpeter, Phys. Rev. 120, 1528 (1960).

[23] D. E. Evans, Plasma Phys. 12, 573 (1970).

[24] W. Kasparek and E. Holzhauer, Phys. Rev. A 27, 1737 (1983).

[25] A. W. DeSilva, T. J. Baig, and H.-J. Kunze, in Proceedings of the Fifth International Symposium on Laser-Aided Plasma Diagnostics (Forschungszentrum, Jülich, 1991), p. 289.

[26] A. W. DeSilva, T. J. Baig, I. Olivares, and H.-J. Kunze, Phys. Fluids B 4, 458 (1992).

[27] M. Arnaud and R. Rothenflug, Astron. Astrophys. Suppl. Ser. 60, 425 (1985).